

## Understanding the electron capture mechanisms during heavy-ion collisions

Manpreet Kaur <sup>1</sup>, Sanjeev Kumar <sup>1</sup> and T. Nandi <sup>2,\*</sup>

<sup>1</sup>*Department of Physics, University Institute of Sciences, Chandigarh University, Gharuan, Mohali, Punjab 140413, India*

<sup>2</sup>*Department of Physics, Ramakrishna Mission Vivekananda Educational and Research Institute, PO Belur Math, Dist Howrah 711202, West Bengal, India*



(Received 7 July 2023; revised 11 October 2023; accepted 1 November 2023; published 17 November 2023)

Besides the direct Coulomb and multiple ionization, ionization caused by the electron capture is found to be a vital mechanism for the x-ray emissions in heavy-ion collisions. This mechanism associated with  $M$ -shell ionization is more complex than that for the  $K$ - and  $L$ -shell ionization and not understood yet. We have developed a theoretical method to understand the  $M$  x-ray production cross sections. Here we have considered both the  $M$ - $K$  and  $M$ - $L$  capture processes of the target atoms by the changed charge state of the projectile ions to witness a good agreement between the present theory and past experiments. We have first verified the present theory with a few representative cases of the carbon, oxygen, and fluorine projectile ions colliding with the lead and bismuth targets at energies ranging from 0.8 to 6.0 MeV/u. Next, we have validated the worth of its predictions through neon ion-induced  $M$  x-ray production of lead and bismuth targets. We believe the current knowledge of the  $M$  x-ray production mechanisms will play a significant role in understanding the different aspects of the heavy-ion collision physics.

DOI: [10.1103/PhysRevA.108.052817](https://doi.org/10.1103/PhysRevA.108.052817)

### I. INTRODUCTION

The study of x rays emitted during ion-atom collision has a wider scope in the different scenarios of physics because they are unique for every element. It has major applications in the field of plasma physics, atomic physics, and particle-induced x-ray emission (PIXE) technique [1–5]. Mostly the proton and alpha beams are used in PIXE experiments [6–13] until now. By employing heavy-ion beams instead of the proton and alpha beams, we can achieve better sensitivity due to higher cross sections [14]. This is not applicable yet due to the wider gap between the experimental and theoretical results. The agreement between the theory and experiment is quite good in the case of the  $K$  shell and quite satisfactory in the case of the  $L$ -shell ionization studies by heavy-ion impacts. As we enter the higher shell like the  $M$  shell, there are complete disagreements observed between the theoretical and experimental results for the heavy-ion collisions, for example, see Refs. [15–17]. It implies that we have a lack of theoretical understanding on the concerned atomic processes involved to date. Direct Coulomb ionization (DCI) plays a dominant role for asymmetric collisions,  $Z_1/Z_2 < 1$ , whereas, for symmetric collisions,  $Z_1/Z_2 \approx 1$ , the multiple ionization (MI) and electron capture (EC) processes in addition to the DCI become increasingly important.  $Z_1$  and  $Z_2$  are the projectile and target atomic numbers, respectively. Chatterjee *et al.* [18,19] have resolved the existing discrepancies between experiment and theory for the  $K$ - and  $L$ -shell ionization. There,

we demonstrated that, besides the MI process,  $K$ - $K$  and  $L$ - $K$  electron-capture processes had played significant roles to sort out such discrepancies. More importantly, the charge state of the heavy projectile ions inside the target must be considered in evaluating the contribution of MI and EC as the inner shell ionization takes place mostly inside the target and barely near the surfaces. We have reported a theoretical methodology to predict the charge state distributions inside (CSD-I) the target. First, this concept has been applied in the  $K$ -shell ionization cases [18]. The same approach has also been applied to study the  $L$ -subshell ionization by considering the MI and the EC along with the DCI by performing a detailed comparison between the experiment and theory [19].

In the present study, we intend to understand the  $M$ -shell ionization in heavy-ion collisions.  $M$ -shell ionization due to  $M$ - $L$  capture is very complex because the  $M$  and  $L$  shells involve five and three subshells, respectively. The  $M$  shell requires three different types of wave functions for describing the system theoretically. As a result, previous studies on  $M$ -shell ionization have not yet achieved a satisfactory level of understanding.

### II. THEORY OF MULTIPLE IONIZATION PHENOMENON (DCI-MI)

The phenomenon of multiple ionization or multiple vacancies in heavy-ion collisions takes place due to strong perturbations. Not only is a vacancy created in the  $M$  shell but also one or more spectator vacancies are created in higher shells also during the heavy-ion collisions. More than one target electron is affected in the majority of the individual collisions. This causes plenty of issues on the Auger, the Coster-Kronig (CK), and the fluorescence yields, as well

\*nanditapan@gmail.com; Previous address: Inter University Accelerator Centre, JNU New Campus, Aruna Asaf Ali Marg, New Delhi-110067, India.

as the transition energies. Thus, the estimation of the values of the different atomic parameters is quite complicated in such circumstances. The theoretical description of multiple ionization is thus quite complicated due to the strong perturbations in the collisions. Various theories have been employed to explain the phenomenon from time to time, for example, the ionization theories like the semiclassical approximation (SCA) and the modified binary-encounter approximation (BEA) in the seventies [20,21] were employed for zero impact parameter heavy-ion collisions only. In the next decade, Lapicki *et al.* [22] proposed an exploratory formula to account for multiple ionization in terms of a classical probability. Sulik *et al.* [23] generalized and extended the simple geometrical model developed for multiple ionization probabilities on the basis of a BEA model to take into account the magnetic substates and nonzero impact parameters during the heavy-ion collisions. The latter was successful in comparing the results with a wide range of experimental data, and no contradictions were found. Furthermore, the Sulik model [23] works in a wider energy range than the Lapicki model [22]. Although the formulation prescribed by Lapicki *et al.* [24] has been used in a few cases, there are some important issues, as discussed below.

Due to the simultaneous multiple ionization, besides the active shell, a vacancy can also be created in higher shells. Nonavailability of electrons in higher shells results in the decrease of the nonradiative transition rate (Auger transition as well as CK transition rate  $f_{ij}$ ), which in turn increases the fluorescence yield  $\omega_i$ . We have to consider these modified values of atomic parameters in order to incorporate the MI effect with DCI. We have taken the  $\omega_i^0$  and  $f_{ij}^0$  values for single-vacancy cases from Chauhan and Puri [25] and then modified them to account for the MI effects according to the prescription of Lapicki *et al.* [24] as follows:

$$\omega_i = \omega_i^0 [1 - P(1 - \omega_i^0)]^{-1}, \quad (1)$$

while the  $f_{ij}$  values for multiple ionization are given by

$$f_{ij} = f_{ij}^0 [1 - P]^2. \quad (2)$$

The ionization probability  $P$  is given by

$$P = q^2 (1 - \beta/4v_1^2) / 2\beta v_1^2. \quad (3)$$

Here,  $\beta = 0.9$ ,  $v_1 = 6.351[E_1(\text{MeV})/M_1(\text{amu})]^{1/2}$  is projectile velocity,  $E_1$  and  $M_1$  are energy and mass of the projectile, respectively, and  $q$  is the charge state of the projectile ion. However,  $q$  has been taken as the atomic number of the projectile ion and incident charge state of the projectile ion in Mehta *et al.* [26] and Lapicki *et al.* [24], respectively. It is noteworthy that Mitra *et al.* [27] has also taken the atomic number of the projectile ions in order to calculate the probability  $P$  using Eq. (3). Therefore, there is no clear idea of  $q$  yet. The right  $q$  value would be the projectile charge state at the point of the collision inside the target between the projectile ion and the target atom. The projectile charge state inside the target can be far different from the incident charge state or atomic number of the projectile [18]. Hence, it is difficult to use Eq. (3) for the multiple ionization probability. On the other hand, the Sulik model [23] does not use the charge state of the projectile ion. Therefore, we use the Sulik model to

estimate the multiple ionization probability for the present work. According to the BEA model of Sulik *et al.* [23], the multiple ionization probability  $P(X_n)$  can be written as a function of a universal scaling parameter  $X_n$  and, thus, the expression for  $P$  in Eq. (3) can be replaced by  $P(X_n)$  [23] as written below:

$$P(X_n) = \frac{X_n^2}{4.2624 + X_n^2 [1 + 0.5 \exp(-X_n^2/16)]}, \quad (4)$$

where  $X_n (= W/n)$  involves the principal quantum number  $n$  of the given shell and a universal scaling variable  $W$  as

$$W = 4 \frac{Z_1}{v_1} V [G(V)]^{1/2}. \quad (5)$$

It denotes a measure of the perturbation strength that characterizes the collision.  $V (=v_1/v_{2s})$  is the scaled projectile velocity,  $v_{2s} [(Z_2 - S_s)/n_2]$  is the orbital electron velocity, and the target shell is characterized by the principle quantum number  $n_2$ .  $S_s$  is the screening constant for the  $s$  orbital. According to the Slater rules [28],  $S_{M_i} = 11.25$  ( $i = 1, 2, 3$ ) and  $S_{M_i} = 21.15$  ( $i = 4, 5$ ). While  $G(V)$  is the BEA scaling function, which is derived from a large number of experiments, its values are tabulated over a large range of  $V$  in McGuire and Richard [21]. In this paper, the values of  $G(V)$  were determined by two methods: (i) the Gerjuoy-Vriens-Garcia approach [29] and (ii) Gryzinski's model [30]. According to McGuire and Richard [21], the Gerjuoy-Vriens-Garcia  $G(V)$  is more accurate than Gryzinski's  $G(V)$  and thus we use the  $G(V)$  of Gerjuoy-Vriens-Garcia to estimate the multiple ionization probability. Note that the DCI is evaluated using the ISICSOO code [31] with  $\omega_i^0$  and  $f_{ij}^0$  [32] already available in the input data of this code. Theoretical approaches of this code can be seen in Batič *et al.* [33]. In this code, the DCI process has been treated perturbatively using first-order perturbation approaches, namely, the plane-wave Born approximation (PWBA) [34]. The standard PWBA approach for DCI was further developed to include the hyperbolic trajectory of the projectile, the relativistic wave functions, and the corrections for the binding-polarization effect. The most advanced approach goes beyond the first-order treatment to include the corrections for the binding polarization effects within the perturbed stationary states (PSS) approximation, the projectile energy loss (E), and Coulomb deflection (C) effects as well as the relativistic (R) description of inner-shell electrons is known as the ECPSSR theory [35]. A brief description of PWBA and ECPSSR formalism is given as standard procedure of the ISICS code in Liu and Cipolla [36]. ECPSSR theory is further modified to replace the PSS effect by a united and separated atom (USA) treatment, which is known as ECUSAR theory [24]. It has also been briefed as an improved version of ISICS later [37]. Therefore we have not repeated them again here.

Instead of DCI with single vacancy we have considered the DCI including the MI contribution, which is calculated using the same code with the  $\omega_i$  and  $f_{ij}$  values as obtained from Eqs. (1), (2), and (4) in place of the  $\omega_i^0$  and  $f_{ij}^0$ . Note that we have taken Dirac-Hartree-Slater (DHS) values for  $\omega_i^0$  and  $f_{ij}^0$  [25]. The change of atomic parameters is done through an input data file, a provision of the program itself.

TABLE I. Representative values of  $J_{ss'}(q)$  and  $K_{ss'}(q)$  (for  $s = 3$  and  $s' = 1$ ) as used in Eq. (7) for  $^{12}\text{C}$  to  $^{20}\text{Ne}$  ions impacting on any target having electrons up to  $n \geq 4$  shell. In the second and third columns, the charge state  $q$  is given along with the elemental ion name in the parentheses.

$q$	5(C), 7(O), 8(F), 9(Ne)	6(C), 8(O), 9(F), 10(Ne)
$J_{ss'}(q)$	1	2
$K_{ss'}(q)$	1	1

III. THEORY OF ELECTRON-CAPTURE PHENOMENON

About 50 years ago Nikolaev [38] developed an expression for evaluating electron capture cross sections in the framework of the Oppenheimer-Brinkman-Kramers (OBK) approach, where the capture taking place from target atoms to projectile ions during heavy-ion collisions. Lapicki and McDaniel [39] modified the cross-section formulation for electron capture from the  $K$  shells of the target atoms to the projectile  $K, L, M$  shell, while the projectiles are taken as the bare ions. In this work, we consider any kind of projectile ions (bare as well as multi-electronic ions) for inner-shell ionization [ $K$  ( $s = 1$ ),  $L$  shell ( $s = 2$ ),  $M$  shell ( $s = 3$ ), etc.] of the target atoms. Here, we give a special emphasis on the electron capture from the  $M$  shell ( $s = 3$ ) of the target atoms, while it takes place in the  $K$  shell ( $s' = 1$ ) and  $L$  subshells ( $s' = 2$ ) of the projectile ions. To do this we have modified the corresponding equation of Ref. [39]. Here, we introduce a factor  $\chi_{ss'}$  in place of two, which is a constant factor for the bare projectile ions, as follows:

$$\sigma_{ss'}^{\text{OBK}} = \frac{2^8 \pi}{5} \frac{n_1^2}{v_1^2} \left( \frac{v_{1s'}}{v_{2s}} \right)^5 \xi_{ss'}^{10}(\theta_s) \frac{\phi_4(t_{ss'}) \chi_{ss'}}{(1 + t_{ss'})^3}. \quad (6)$$

Here, the subscripts 1 and 2 refer to the projectile and target, respectively. The projectile shell is characterized by the quantum number  $n_1$  and the orbital velocity of the electron in the projectile is given as  $v_{1s'} (=z_1/n_1)$ . Here the parameter  $\chi_{ss'}$  plays an important role in the  $ss'$  electron-capture processes and is given by

$$\chi_{ss'} = \sum_q \frac{F(q) J_{ss'}(q)}{K_{ss'}(q)}. \quad (7)$$

For  $\chi_{ss'=1}$ ,  $q$  corresponds to bare and H-like projectile ions only, i.e., while vacancies exist in the  $K$  shell. Whereas for  $\chi_{ss'=2}$ ,  $q$  spans over bare to  $F$ -like projectile ions. The quantities  $F(q)$  is the charge state fraction of projectile ion inside the target element for the charge state  $q$ ,  $J_{ss'}(q)$  = the number of vacancies present in the  $s'$  shell of the projectile for capturing electrons from the  $s$  shell of the target atom corresponding to a particular charge state  $q$  and  $K_{ss'}(q)$  is a constant factor depending on the number of subshells in the  $s'$  shell of the projectile participating in the capture, which is determined on the consideration of ionization energies. The ionization energies of the states  $2p_{3/2}$ ,  $2p_{1/2}$ , and  $2s_{1/2}$  for C, O, F, and Ne are in increasing order. Thus, it is simple to find  $J_{ss'}(q)$  and  $K_{ss'}(q)$  for any  $q$  and any projectiles. The values of  $J_{ss'}(q)$  and  $K_{ss'}(q)$  for (i)  $s = 3$  and  $s' = 1$  and (ii)  $s = 3$  and  $s' = 2$  are

TABLE II. Representative values of  $J_{ss'}(q)$  and  $K_{ss'}(q)$  (for  $s = 3$  and  $s' = 2$ ) as used in Eq. (7) for  $^{12}\text{C}$  to  $^{20}\text{Ne}$  ion impacting on any target having electrons up to  $n \geq 4$  shell.

For $^{12}\text{C}$ beam										
$q$	1	2	3	4	5	6				
$J_{ss'}(q)$	1	2	3	4	4	4				
$K_{ss'}(q)$	1	1	2	2	2	2				
For $^{16}\text{O}$ beam										
$q$	1	2	3	4	5	6	7	8		
$J_{ss'}(q)$	1	2	3	4	5	6	6	6		
$K_{ss'}(q)$	1	1	2	2	3	3	3	3		
For $^{19}\text{F}$ beam										
$q$	1	2	3	4	5	6	7	8	9	
$J_{ss'}(q)$	1	2	3	4	5	6	7	7	7	
$K_{ss'}(q)$	1	1	1	2	2	3	3	3	3	
For $^{20}\text{Ne}$ beam										
$q$	1	2	3	4	5	6	7	8	9	10
$J_{ss'}(q)$	1	2	3	4	5	6	7	8	8	8
$K_{ss'}(q)$	1	1	1	1	2	2	3	3	3	3

given in Tables I and II, respectively for the projectiles C, O, F, and Ne.

The reduced binding energy  $\theta_s$  of the target electron which is being captured by the projectile ion [40] is defined as

$$\theta_s = \frac{\text{Observed binding energy}}{v_{2s}^2 \times 13.6}. \quad (8)$$

Since  $\theta_s$  varies with the subshells, we get  $\sigma_{ss'}^{\text{OBK}}$  different for different subshells from Eq. (6). The parameter  $\xi_{ss'}(\theta_s)$  in Eq. (6) is defined by Lapicki and McDaniel [39]:

$$\xi_{ss'}(\theta_s) = \frac{v_{2s}}{\sqrt{[v_{1s'}^2 + q_{ss'}^2(\theta_s)]}}, \quad (9)$$

where  $q_{ss'}(\theta_s)$  measures the momentum transfer in the capture process as follows:

$$q_{ss'}(\theta_s) = \frac{v_1}{2} + \frac{v_{2s}^2 \theta_s - v_{1s'}^2}{2v_1}. \quad (10)$$

In Eq. (6), the function  $\phi_4(t_{ss'})$  is approximated to within 2% by

$$\phi_4(t_{ss'}) = \frac{1}{1 + 0.3t_{ss'}} \quad (11)$$

for  $t_{ss'} < 3$ . The variable  $t_{ss'}$  is expressed as

$$t_{ss'} = (1 - \theta_s) \xi_{ss'}^2(\theta_s). \quad (12)$$

The projectile-velocity-dependent electron-capture cross section can be written according to Lapicki and McDaniel [39]. For low-velocity ions ( $v_1 \ll v_2$ ), the cross section  $\sigma_{(<)}^{\text{OBK}}$  is given by

$$\sigma_{ss'(<)}^{\text{OBK}} = C_{ss'} \sigma_{ss'}^{\text{OBK}} [\xi_{ss'}(\lambda_{ss'} \theta_s), \lambda_{ss'} \theta_s], \quad (13)$$

where  $\lambda_{ss'}$  is the binding-energy correction term for target  $M$  shell and  $C_{ss'}$  is the Coulomb deflection factor, which is caused

by the united atom formation in low velocity.  $\lambda_{ss'}$  is described as follows:

$$\lambda_{ss'} = 1 + \frac{2Z_1}{(Z_2 - S_s)\theta_s}, \quad (14)$$

and the factor  $C_{ss'}$  is given by Lapicki and McDaniel [39]:

$$C_{ss'} = \exp[-\pi D q_{ss'}(\lambda_{ss'}\theta_s)]. \quad (15)$$

The half-distance ( $D = Z_1 Z_2 / M v_1^2$ ) of the closest approach in a head-on collision is approximated by the reduced mass ( $M^{-1} = M_1^{-1} + M_2^{-1}$ ) of the scattering system, where  $M_1$  and  $M_2$  are the atomic mass of the projectile and target, respectively. The binding effect reduces the ionization cross section by effectively increasing  $\theta_s$  to  $\lambda_{ss'}\theta_s$ .

Whereas the electron-capture cross sections for high velocity ions ( $v_1 \gg v_2$ ) ( $\sigma_{(>)}^{\text{OBK}}$ ) takes the form

$$\sigma_{ss'(>)}^{\text{OBK}} = \frac{1}{3} \sigma_{ss'}^{\text{OBK}} [\xi_{ss'}(\lambda_{ss'}\theta_s), \lambda_{ss'}\theta_s], \quad (16)$$

and for the intermediate velocity range ( $=v_1 \approx v_2$ ) the capture cross section ( $\sigma_{(\approx)}^{\text{OBK}}$ ) takes the following form:

$$\sigma_{ss'(\approx)}^{\text{OBK}} = \frac{[\sigma_{ss'(<)}^{\text{OBK}} \sigma_{ss'}^{\text{OBK}}]}{[\sigma_{ss'}^{\text{OBK}} + 2\sigma_{ss'(<)}^{\text{OBK}}]}. \quad (17)$$

In the present study, velocity ( $v_1$ ) of the projectile ions lies in the range of 5.65 to 15.55 a.u. Whereas electron orbital velocity in the  $M$  shell of the lead target is about 20.28 to 23.58 a.u. and 20.61 to 23.91 a.u. for the bismuth target. So for obtaining the ML electron-capture cross section we have used the formulation of Eq. (13) applicable to the low-velocity regime ( $v_1 \ll v_2$ ).

To compare the theoretical predictions of total  $M$ -shell ionization cross sections with the experimentally obtained total  $M$ -shell production cross section of Refs. [15–17], we need to convert the theoretically calculated total ionization cross section to the total production cross section. This conversion is a routine practice and has now been incorporated in the ISICS00 code [31]. However, converting the ionization contribution due to electron capture (IC) to the  $M$  x-ray production cross section due to capture (XC) is to be included and is out of the scope of the ISICS00 code. We have made use of  $M$ -subshell fluorescence yields  $\omega_i$ ,  $i = 1-5$  in the total x-ray production cross section due to capture  $\sigma_M^{\text{XC}}(\text{tot})$  as follows:

$$\sigma_M^{\text{XC}}(\text{tot}) = \omega_1 \sigma_{M_1}^{\text{IC}} + \omega_2 \sigma_{M_2}^{\text{IC}} + \omega_3 \sigma_{M_3}^{\text{IC}} + \omega_4 \sigma_{M_4}^{\text{IC}} + \omega_5 \sigma_{M_5}^{\text{IC}}. \quad (18)$$

In the present case, ionization cross section due to capture in  $M_i$  subshell  $\sigma_{M_i}^{\text{IC}}$  is written as  $\sigma_{M_i}^{\text{IC}} = \sigma_{M_i(<)}^{\text{OBK}}$ , where  $i = 1-5$ . Note that  $\sigma_{M_i(<)}^{\text{OBK}}$  is obtained from Eq. (13) if we write  $s = M_i$  in place of  $s$  and omit  $s'$  from  $\sigma_{ss'(<)}^{\text{OBK}}$ .  $\omega_1$  to  $\omega_5$  are the same values as used for evaluating DCI plus MI. Hence, the total  $M$  x-ray production cross section  $\sigma_M^{\text{X}}(\text{tot})$  is given by

$$\sigma_M^{\text{X}}(\text{tot}) = \sigma_{\text{DCI-MI}}^{\text{X}}(\text{tot}) \text{ from ISICS00 code} + \sigma_M^{\text{XC}}(\text{tot}). \quad (19)$$

Here, the first term on the right-hand side gives a measure of DCI and MI and the second term accounts for the  $M$  x-ray production cross section due to electron capture.

#### IV. MEAN CHARGE STATE AND CHARGE STATE DISTRIBUTION OF THE PROJECTILE IONS INSIDE THE TARGET

Although a monochromatic ion beam is passed through the target, ion-solid interaction leads to a certain charge exchange inside the target. It leads to a mean charge state ( $q_m^i$ ) inside the target, which is measured along with the charge state distribution by an x-ray spectroscopy technique [43].  $q_m^i$  so measured can be far different from the mean charge state if measured using a device such as a dipole magnet placed outside the target. We call this mean charge state outside the target  $q_m^o$ . This difference increases with heavier ions, as seen from a series of our measurements which are yet to be published. The reason for this difference is the fact that the mean charge state through a plasma target is higher than that through any solid target [44]. Interestingly, when the projectile ions are accompanied with many electrons and are allowed to pass through a thin solid foil, such ion-solid collisions lead to a tenuous plasma inside the foil, called a beam-foil plasma [1]. Hence, projectile ions through a beam-foil plasma give rise to higher charge states than  $q_m^o$ . Conversion from  $q_m^i$  to  $q_m^o$  takes place due to electron capture from the exit surface of the thin solid target. This fact is evinced by Sharma and Nandi [45].

$q_m^o$  can be estimated by using the empirical model of Schiwietz and Grande [42] (SGM), as given below:

$$q_m^o = Z_1 \frac{12x_o + x_o^4}{0.07/x_o + 6 + 0.3x_o^{0.5} + 10.37x_o + x_o^4}, \quad (20)$$

with

$$x_o = \left[ \frac{1}{1.68} \frac{v_1}{v_o} Z_1^{-0.52} Z_2^{(-0.019Z_1^{-0.52}v_1/v_o)} \right]^{(1+1.8/Z_1)}, \quad (21)$$

where  $v_o$  is the Bohr velocity ( $2.19 \times 10^6$  m/s). On the other hand, to obtain the  $q_m^i$ , we employ the empirical formula based on the Fermi gas model (FGM) [41]:

$$q_m = Z_1 \left( 1 - \frac{v_F}{v_1} \right), \quad (22)$$

where  $v_F$  is the Fermi velocity of target electrons. For the present case,  $v_F$  is estimated from Ref. [46]. Projectile electron stripping is only allowed in the FGM when  $v_1 > v_F$  and then maximum stripping occurs for  $v_1 \gg v_F$ . Furthermore, this formula is useful only for the foil thickness  $\geq$  the equilibrium target-foil thickness. Note that the  $q_m^i$  can also be the target ionization by the electron-capture process. However, it is restricted for the limited ions as per the constraints with the code [47]. A little detail can be seen in Chatterjee *et al.* [18].

In the second step, to obtain the charge state fractions  $F(q)$  the  $q_m^i$  values are substituted for  $q_m$  in the Lorentzian charge state distribution [43] as follows:

$$F(q) = \frac{1}{\pi} \frac{\frac{\Gamma}{2}}{(q - q_m)^2 + \left(\frac{\Gamma}{2}\right)^2} \text{ and } \sum_q F(q) = 1, \quad (23)$$

where distribution width  $\Gamma$  is taken from Novikov and Teplova [48] as follows:

$$\Gamma(x) = C \{ 1 - \exp[-(x)^\alpha] \} [ 1 - \exp(-(1-x)^\beta) ], \quad (24)$$

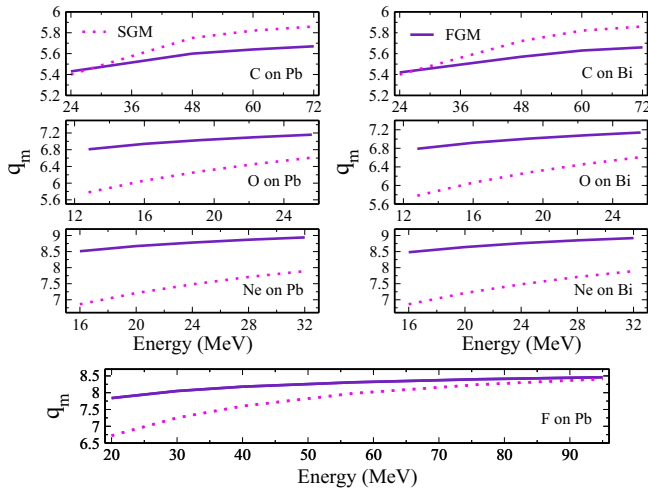


FIG. 1. Comparison of theoretical mean charge states ( $q_m$ ) of  $^{12}\text{C}$ ,  $^{16}\text{O}$ ,  $^{19}\text{F}$ , and  $^{20}\text{Ne}$  ion beams as a function of beam energies.  $q_m$  inside the target ( $q_m^i$ ) differs from  $q_m$  outside the target ( $q_m^o$ ).  $q_m^i$  and  $q_m^o$  are predicted by the Fermi gas model (FGM) [41] and the Schiwietz-Grande model (SGM) [42], respectively.

where  $x = q_m/Z_1$ ,  $\alpha = 0.23$ ,  $\beta = 0.32$ , and  $C = 2.669 - 0.0098Z_2 + 0.058Z_1 + 0.00048Z_1Z_2$ .

Note that both the projectile-energy-dependent  $q_m^i$  and  $F(q)$  given above can now be used for estimating the atomic parameters in the presence of multiple vacancies and electron-capture cross sections needed to evaluate the  $M$  x-ray production cross sections.

## V. RESULTS AND DISCUSSIONS

The mean charge state outside the solid target does not have any relevance in inner-shell ionization of the target. We bring it here to have a contrast so that a better understanding of the charge-exchange phenomenon inside the target can be possible. To showcase the difference of the projectile charge state inside ( $q_m^i$ ) and outside ( $q_m^o$ ) the target, we have displayed  $q_m^i$  as well as  $q_m^o$  as a function of the projectile energy in Fig. 1. We can see an unusual trend here, for instance, at 24 MeV for  $^{12}\text{C}$ , the mean charge state inside the target is slightly larger than that outside the target, and increasing the energy, a reverse relationship is observed. The reverse relationship is not at all physically possible, but the two mean charge states may converge at the higher energies because of very low electron-capture cross section at the high energies, as observed in case of  $^{19}\text{F}$  on a Pb target. In ion-solid collisions, the charge-exchange process is complicated and we have found that Eq. (20) is not accurate enough to describe the charge state outside the target for any projectiles spanning from light to heavy ions. The main reason is that Eq. (20) is a function of a scaling variable  $x_0$  and  $x_0$  is a function of  $Z_1$ ,  $Z_2$ , and  $v_1$ . The choice of  $x_0$  is not good enough to constitute a single equation that can represent all the ions. We noticed that Eq. (20) overestimates the measured data for the light ions. The above-mentioned fact with  $^{12}\text{C}$  ions is in fact due to this. With this  $x_0$ , at least three to four equations are required to represent all the elemental ions in the periodic table instead

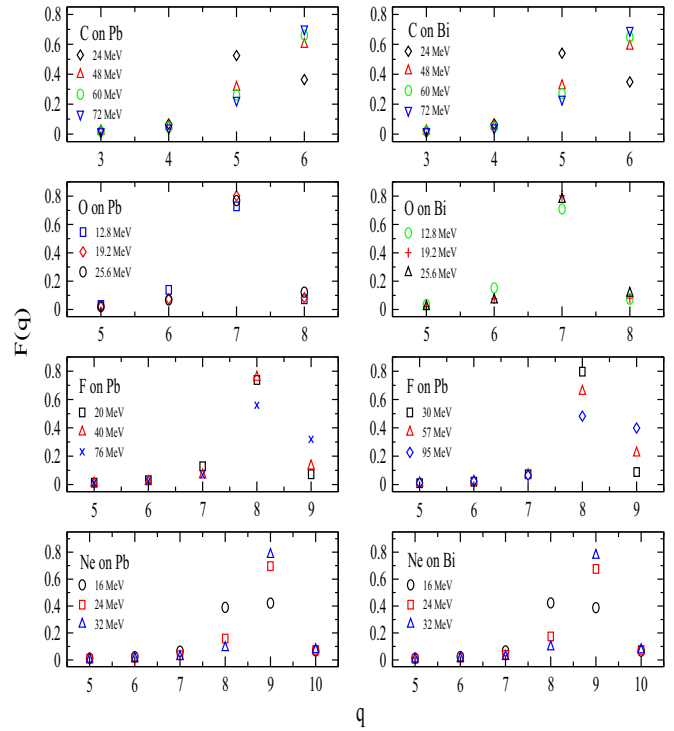


FIG. 2. Charge state distributions inside different targets for different ion beams at various beam energies: Charge state fractions  $F(q)$  for a particular charge state  $q$  are calculated by using the Lorentzian distribution with the distribution width from Novikov and Teplova [48] and  $q_m$  from the FGM model [41] at each beam energy.

of only one equation. We have been working on this issue for quite some time and a paper is being prepared for publication.

$q_m^i$  is governed by the ion-solid interaction at the bulk of the target.  $q_m^i$  is changed a lot by the interaction of the projectile ions with the solid surface [45,49,50] and the resulted charge state is nothing but the  $q_m^o$ . The  $F(q)$  values obtained using Eq. (23) are plotted as a function of  $q$  in Fig. 2. This curve is known as the charge state distribution (CSD), which gives us an idea of the type of EC taking place, i.e.,  $M$ - $K$  or  $M$ - $L$  capture. From Fig. 2 it is clear that, for C, O, and F projectile ions, vacancies appear up to the  $K$  shell. Thus, both  $M$ - $K$  and  $M$ - $L$  captures are possible for all the projectile ions.

We notice from Fig. 1 that there is a large difference between the mean charge state inside and outside the target for all the ions except carbon, as discussed above. Thus the CSD outside the target cannot replace the CSD inside the target, which is responsible for the inner-shell ionization process happening inside the target. The CSD inside the target obtained from FGM for the seven cases is shown in Fig. 2. These charge state fractions obtained indicate that both  $M$ - $K$  and  $M$ - $L$  electron capture are possible for all the projectiles. Furthermore, these charge state fractions are used to estimate the concerned electron-capture contributions.

To test the above theoretical methodologies for the MI and EC applicable to the  $M$ -shell, we have made use of the experimental results of Singh *et al.* [15] and Gorlachev *et al.* [16]. They used the carbon and oxygen projectile ions on lead and bismuth targets in the energy range of 24–72 and

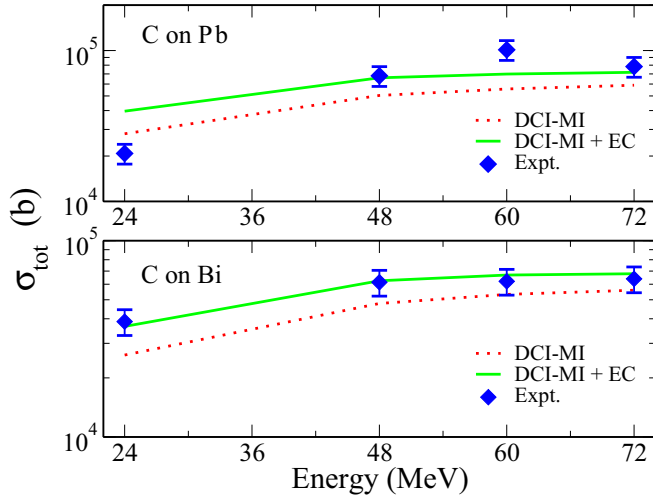


FIG. 3. Total  $M$ -shell production cross sections [ $\sigma_{\text{tot}}$  is same as  $\sigma_M^X(\text{tot})$ ] in the units of barns (b) for Pb and Bi targets bombarded by the  $^{12}\text{C}$  ions as a function of ion-beam energies: Experimental [15] data have been compared with various theoretical cross sections. ECPSSR cross sections (DCI) using the ISICSOO code [31] have been corrected with the formalism of Lapicki *et al.* [24] (DCI-MI), while the  $M$  x-ray cross sections due to electron capture (EC) have been calculated using the present theory.

12–26 MeV, respectively, and fluorine beam on lead target in the energy range of 20–95 MeV.

We intend to compare the total  $M$  x-ray production cross sections with the theoretical predictions at different stages, viz., the direct Coulomb ionization including MI (DCI-MI), and DCI-MI + EC. For DCI-MI, we used ECPSSR theory (ECPSSR and ECUSAR give almost the same results for the asymmetric collisions) because it gives the best representation for the  $K$ - and  $L$ -shell ionization cross section as a function of beam energies, as shown in our recent studies [18,19]. Next, to estimate the effect of MI and EC in the  $M$  x-ray

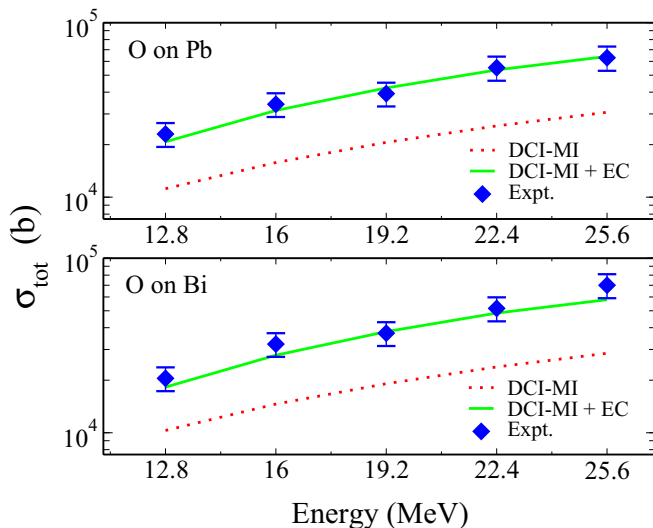


FIG. 4. Same as Fig. 3, but an  $^{16}\text{O}$  ion beam is used for the experiment [16].

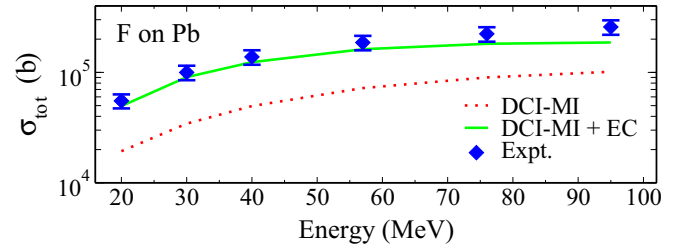


FIG. 5. Same as Fig. 3, but a  $^{19}\text{F}$  ion beam is used for the experiment [15].

production cross section, we need to have a clear idea of the projectile charge state distribution inside the target, as shown in Fig. 2. We compare the C-ion-induced  $M$  x-ray emission phenomena in Fig. 3. Here, we notice that the DCI-MI values are quite smaller than the experimental figures, whereas good agreement is attained by taking electron capture into consideration. In other words, inclusion of the electron-capture cross sections  $\sigma_{EC}$  along with the DCI-MI, the total  $M$ -shell production cross section  $\sigma_M^X(\text{tot})$  leads to a good agreement with the measured  $\sigma_M^X(\text{tot})$  for the lead target [15]. Whereas this agreement is found to be excellent in case of the bismuth target, as compared in Fig. 3. This is not at all a sole example. The present theoretical approach is further verified with the O- and F-ion induced  $M$  x-ray emission phenomena, as shown in Figs. 4 and 5. In Fig. 4, we see an excellent agreement between the present theory and experiment. The scenario is not bad at all for the fluorine-induced lead target also (Fig. 5). It thus implies that the atomic parameters with single vacancy in the  $M$ -shell [25] used to undertake multiple ionization effects as well as to convert theoretical ionization cross sections to production ones are good.

We have verified the present theory through different heavy-ion collisions:  $^{12}\text{C}$  and  $^{16}\text{O}$  beams on Pb and Bi targets and  $^{19}\text{F}$  beam on a Pb target. These experiments were done at different laboratories and at various energy ranges. Therefore, this thorough verification itself validates the reliability of the theory. Nevertheless, we incorporate another set of

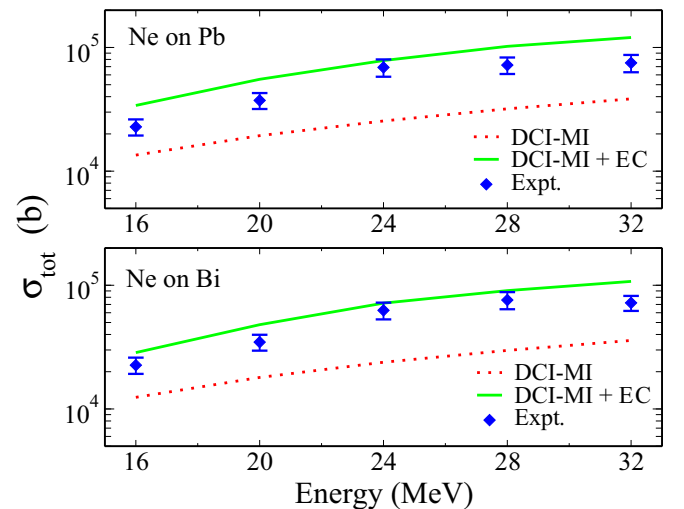


FIG. 6. Same as Fig. 3, but a  $^{20}\text{Ne}$  ion beam is used for the experiment [17].

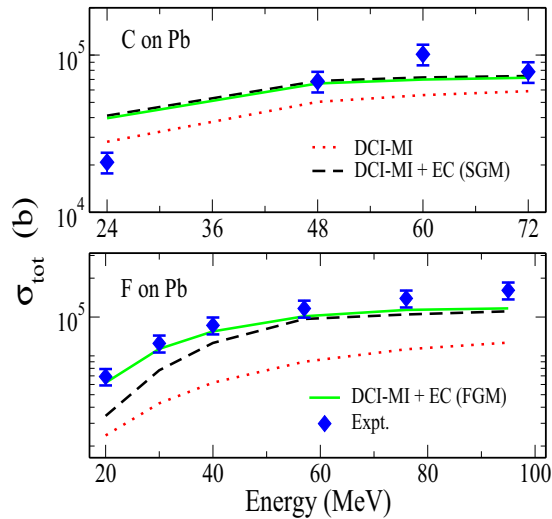


FIG. 7. We show the difference between the  $M$  x-ray production cross sections by considering electron capture with  $q_m^o$  along with  $q_m^i$  for two projectiles: carbon and fluorine ions on a Pb target.

comparison on two collision systems ( $^{20}\text{Ne}$  beam with lead and bismuth targets), as shown in Fig. 6, and find a satisfactory level of agreement in these systems also. Hence, we believe the present theory gives us a fair level of understanding for  $M$ -shell ionization by heavy-ion impacts.

We mentioned above the difference between  $q_m^o$  and  $q_m^i$ . Now let us apply the two mean charge states  $q_m^i$  and  $q_m^o$  in describing the electron capture. We can clearly see the similar difference in total  $M$  x-ray production cross sections in Fig. 7. The difference between the  $q_m^i$  and  $q_m^o$  for C ions is small (Fig. 1); a similar difference is seen here, too. Whereas the difference between the two is large in the low-energy side for F ions, a similar difference is seen here, too, and is reduced in the higher-energy side.

## VI. CONCLUSION

Multiple ionization and electron capture are found to be vital mechanisms for  $K$  and  $L$  x-ray emissions along with the direct Coulomb ionization in heavy-ion collisions. Naturally, one may think similar mechanisms may also be significant for  $M$  x-ray emissions also. We see that the DCI-MI values alone are not enough to match the experimental figures. To study actual fact we have developed a theoretical method that studies the combined effects of direct Coulomb ionization including the multiple ionization and electron capture step by step. We have verified the present theory with five collision systems and then validated such a theory with the two collision systems. Remarkably, this theoretical approach has helped us to resolve the longstanding problem between the theories and experiments prevalent in  $M$ -shell ionization physics by heavy-ion impacts.

- [1] P. Sharma and T. Nandi, *Phys. Plasmas* **23**, 083102 (2016).
- [2] T. Satoh, *Int. J. PIXE* **25**, 147 (2015).
- [3] N. A. Dyson and N. A. Dyson, *X-Rays in Atomic and Nuclear Physics* (Cambridge University Press, Cambridge, UK, 2005).
- [4] M. Antoszewska-Moneta, R. Brzozowski, and M. Moneta, *Eur. Phys. J. D* **69**, 77 (2015).
- [5] A. W. Gillespie, C. L. Phillips, J. J. Dynes, D. Chevrier, T. Z. Regier, and D. Peak, *Adv. Agron.* **133**, 1 (2015).
- [6] T. B. Johansson, R. Akselsson, and S. A. Johansson, *Nucl. Instrum. Methods* **84**, 141 (1970).
- [7] A. Bertol, R. Hinrichs, and M. Vasconcellos, *Nucl. Instrum. Methods Phys. Res. Sect. B* **363**, 28 (2015).
- [8] J. Garcia, *Phys. Rev. A* **1**, 280 (1970).
- [9] D. Joseph, S. N. Rao, and S. Kailas, *Mapana J. Sci.* **12**, 1 (2013).
- [10] X. Zhou, Y. Zhao, R. Cheng, Y. Wang, Y. Lei, X. Wang, and Y. Sun, *Nucl. Instrum. Methods Phys. Res. Sect. B* **299**, 61 (2013).
- [11] J. Miranda, G. Murillo, B. Méndez, J. López-Monroy, J. Aspiazú, P. Villaseñor, J. C. Pineda, and J. Reyes-Herrera, *Nucl. Instrum. Methods Phys. Res. Sect. B* **316**, 113 (2013).
- [12] J. Miranda and G. Lapicki, *At. Data Nucl. Data Tables* **100**, 651 (2014).
- [13] H. Mohan, A. K. Jain, M. Kaur, P. S. Singh, and S. Sharma, *Nucl. Instrum. Methods Phys. Res. Sect. B* **332**, 103 (2014).
- [14] R. Siegele, D. D. Cohen, and N. Dytlewski, *Nucl. Instrum. Methods Phys. Res. Sect. B* **158**, 31 (1999).
- [15] Y. P. Singh, D. Misra, U. Kadhane, and L. C. Tribedi, *Phys. Rev. A* **73**, 032712 (2006).
- [16] I. Gorlachev, N. Gluchshenko, I. Ivanov, A. Kireyev, S. Kozin, A. Kurakhmedov, A. Platov, and M. Zdorovets, *Nucl. Instrum. Methods Phys. Res. Sect. B* **381**, 34 (2016).
- [17] I. Gorlachev, N. Gluchshenko, I. Ivanov, A. Kireyev, M. Krasnopyorova, A. Kurakhmedov, A. Platov, Y. Sambayev, and M. Zdorovets, *Nucl. Instrum. Methods Phys. Res. Sect. B* **448**, 19 (2019).
- [18] S. Chatterjee, P. Sharma, S. Singh, M. Oswal, S. Kumar, C. C. Montanari, D. Mitra, and T. Nandi, *Phys. Rev. A* **104**, 022810 (2021).
- [19] S. Chatterjee, S. Kumar, S. Kumar, M. Oswal, B. Mohanty, D. Mehta, D. Mitra, A. Mendez, D. Mitnik, C. Montanari *et al.*, *Phys. Scr.* **97**, 045405 (2022).
- [20] J. Hansen, *Phys. Rev. A* **8**, 822 (1973).
- [21] J. H. McGuire and P. Richard, *Phys. Rev. A* **8**, 1374 (1973).
- [22] G. Lapicki, R. Mehta, J. L. Duggan, P. M. Kocur, J. L. Price, and F. D. McDaniel, *Phys. Rev. A* **34**, 3813 (1986).
- [23] B. Sulik, I. Kádár, S. Ricz, D. Varga, J. Végh, G. Hock, and D. Berényi, *Nucl. Instrum. Methods Phys. Res. Sect. B* **28**, 509 (1987).
- [24] G. Lapicki, G. A. V. Murty, G. J. Raju, B. S. Reddy, S. B. Reddy, and V. Vijayan, *Phys. Rev. A* **70**, 062718 (2004).
- [25] Y. Chauhan and S. Puri, *At. Data Nucl. Data Tables* **94**, 38 (2008).
- [26] R. Mehta, H. L. Sun, D. K. Marble, J. L. Duggan, F. D. McDaniel, and G. Lapicki, *J. Phys. B: At. Mol. Opt. Phys.* **28**, 1187 (1995).

- [27] D. Mitra, M. Sarkar, D. Bhattacharya, S. Santra, A. Mandal, and G. Lapicki, *Nucl. Instrum. Methods Phys. Res. Sect. B* **268**, 450 (2010).
- [28] J. C. Slater, *Phys. Rev.* **36**, 57 (1930).
- [29] E. Gerjuoy, *Phys. Rev.* **148**, 54 (1966).
- [30] M. Gryziński, *Phys. Rev.* **138**, A336 (1965).
- [31] M. Batič, M. G. Pia, and S. J. Cipolla, *Comput. Phys. Commun.* **184**, 2232 (2013).
- [32] J. L. Campbell, *At. Data Nucl. Data Tables* **85**, 291 (2003).
- [33] M. Batič, M. G. Pia, and S. J. Cipolla, *Comput. Phys. Commun.* **183**, 398 (2012).
- [34] B.-H. Choi, E. Merzbacher, and G. Khandelwal, *At. Data Nucl. Data Tables* **5**, 291 (1973).
- [35] W. Brandt and G. Lapicki, *Phys. Rev. A* **23**, 1717 (1981).
- [36] Z. Liu and S. J. Cipolla, *Comput. Phys. Commun.* **97**, 315 (1996).
- [37] S. J. Cipolla, *Comput. Phys. Commun.* **176**, 157 (2007).
- [38] V. S. Nikolaev, *Sov. Phys.-JETP* **24**, 847 (1967).
- [39] G. Lapicki and F. D. McDaniel, *Phys. Rev. A* **22**, 1896 (1980).
- [40] W. Brandt and G. Lapicki, *Phys. Rev. A* **10**, 474 (1974).
- [41] W. Brandt, R. Laubert, M. Mourino, and A. Schwarzschild, *Phys. Rev. Lett.* **30**, 358 (1973).
- [42] G. Schiwietz and P. L. Grande, *Nucl. Instrum. Methods Phys. Res. Sect. B* **175-177**, 125 (2001).
- [43] P. Sharma and T. Nandi, *Phys. Lett. A* **380**, 182 (2016).
- [44] G. D. Alton, R. A. Sparrow, and R. E. Olson, *Phys. Rev. A* **45**, 5957 (1992).
- [45] P. Sharma and T. Nandi, *Phys. Rev. Accel. Beams* **22**, 034501 (2019).
- [46] C. Nave, Fermi level and Fermi function-hyperphysics concepts, <http://hyperphysics.phy-astr.gsu.edu/hbase/Tables/fermi.html>.
- [47] E. Lamour, P. D. Fainstein, M. Galassi, C. Prigent, C. A. Ramirez, R. D. Rivarola, J.-P. Rozet, M. Trassinelli, and D. Vernhet, *Phys. Rev. A* **92**, 042703 (2015).
- [48] N. V. Novikov and Y. A. Teplova, *Phys. Lett. A* **378**, 1286 (2014).
- [49] T. Nandi, *Astrophys. J.* **673**, L103 (2008).
- [50] G. Sharma, N. K. Puri, P. Kumar, and T. Nandi, *Europhys. Lett.* **120**, 63002 (2017).